ACS OMEGA

Open Access

http://pubs.acs.org/journal/acsodf

Article

Molecular Insights into the CO_2 Mineralization Process with Tricalcium Silicate

Erchao Li, Jianan Zheng, Junjie Lin, Tao Wang, Kun Luo,* and Jianren Fan

Cite This: *ACS Omega* 2024, 9, 46237−46246

Read Online

ACCESS | Metrics & More | Article Recommendations

ABSTRACT: CO_2 mineralization, a pivotal technology in CO_2 capture, storage, and utilization, promises to convert industrial waste into valuable industrial products. However, the intricate reaction mechanism and rate-limiting process remain inadequately elucidated. The suitable reaction conditions should be clarified when designing industrial produce. In this study, we comprehensively examined the reaction kinetics and conversion rates of C_3S under varying conditions and degrees of dispersion by reactive molecular dynamics simulation. Furthermore, we set up a sophisticated model depicting C_3S encased within a water film, mirroring its prevalent configuration in moist environments. The results show that the reaction is fast when the temperature is 328 K. The conversion rate tends to decrease under elevated pressure when it is higher than 1.0 MPa, while the temperature has a minimal impact. Fragmentation of solid waste can increase the degree of dispersion, disrupting the crystal structure and expanding the reaction surface area, thereby accelerating the reaction. The presence of a water film impedes mass transfer, consequently reducing the reaction speed. The present study sheds light on the reaction mechanism of the CO_2 mineralization process.

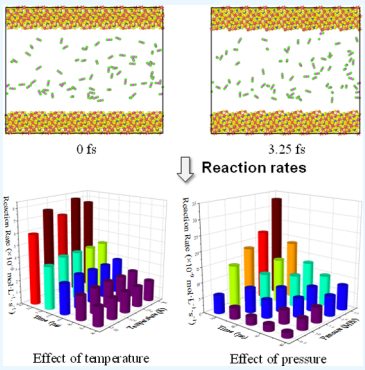

1. INTRODUCTION

Large amounts of carbon dioxide emissions exacerbate the greenhouse effect.[1] Thereby, many issues come into being, such as climate change, iceberg melting,[2] sea level rise, and so on. Carbon capture, storage, and utilization are necessary approaches to removing CO_2 on a large scale.[3] CO_2 mineralization technology refers to the reaction of CO_2 and natural mineral/industrial waste. 4.02 Gt CO_2 can be captured by industrial alkaline waste.[4] Micrometer $CaCO_3$ with high-value attachment can be produced during this process.[5,6] CO_2 mineralization technology is of great sequential potential,[7] and carrying out new CO_2 mineralization technologies can contribute to turning waste into industrial resources and achieving the goal of carbon neutrality.

Plenty of experimental efforts have been made to study CO_2 mineralization technologies. For example, Reddy et al.[8] conducted experiments on the mineralization of fly ash, a byproduct of coal combustion, using a fluid bed reaction container. The results revealed that unseparated CO_2 and SO_2 could be mineralized by fly ash, with the reaction completed within just a few minutes. Helwani et al.[9] discovered that in situ mineralization in a power plant was more effective than geologic sequestration for carbon capture and storage. Polettini et al.[10] researched the impact of temperature, pressure, and CO_2 concentration on conversion rate and found the reaction condition where the conversion of CO_2 was the highest. However, the previous works did not understand the mineralization reaction on a mechanism level. Some researchers found that $CaCO_3$ could be produced by steel slag carbonation.[11,12] Besides, ammonium salt contributed to the diffusion of Ca^{2+}, and the liquid-to-solid ratio influenced the diffusion rate greatly.[12] However, this experiment did not reveal mineralization reaction mechanisms. C_3S is the active phase in industrial waste. The crystal structure of C_3S is a tetrahedron whose center is a silicon atom coordinated by oxygen atoms.[13] The silicon-oxygen tetrahedrons are connected by covertex, coedge, and coface, whose structure is unstable. In the C_3S crystal, the coordination number of Ca−O is large and the force between atoms is weak. These features make it easy to be ruined by CO_2 molecules. Thus, a mineralization reaction takes place. Reaction dynamics information can be obtained from the above experiments. Nevertheless, the experimental method can only understand the mineralization process from the macro level, cannot reveal the mechanism of mineralization reaction from the microscale, and is only confined to the limited operating conditions, which hinders the further development of mineralization technologies.

Numerical simulation provides a repeatable and cost-effective alternative to the experimental method, with the

Received: July 31, 2024
Revised: October 20, 2024
Accepted: October 22, 2024
Published: November 11, 2024

rapid development of numerical algorithms and computer hardware. Molecular dynamics (MD) is gradually emerging as a mainstream high-fidelity method for investigating mineralization processes, attracting widespread attention from researchers. For example, Zhao et al.[14] researched the carbonation process on the surface of γ-C2S and found that chemical adsorption was far stronger than physical adsorption. HCO_3^- deprotonation took place, and a more stable structure formed. However, this process needed to jump over the energy barrier. Mutisya and Kalinichev[15] pointed out that the mutual influence of cement and water contributed to water film formation on the solid surface and hindered CO_2 diffusion to the solid surface. The reaction rate depended on the structure of the cement holes and the water layer. However, constrained by the numerous computing resource demands of ab initio MD simulation, this research did not detect the solution process of the calcium salt. This drawback could be overcome by reactive molecular dynamics (RMD) simulation. Zare et al.[16] pointed out that the mineral surface was covered by a nanometer-scale width water layer during the mineralization process under moisture conditions. The reverse proton transfer phenomenon coincided with the results detected by in situ spectroscopy. Qin et al.[17] studied the calcium carbonation nucleation process during the mineralization process by reactive and classic MD simulation and found that the results of the dynamic properties computed by RMD simulation were consistent with experiment results than classic MD. Wang et al.[18] examined the role of H_2O during the carbonation process and pointed out that water-induced adsorption of CO_2 in the diffusion control stage in low temperatures. The diffusion of ions and CO_2 molecules became more tense, and the thickness of the product layer increased with water. Dai et al.[19] investigated the mineralization reaction between CO_2 and illite and discovered the protonation process of nonbridging oxygen atoms. Cations could reach the liquid area through cube and tetrahedron space and combine with HCO_3^- to form carbonation salt. They hold the point of view that RMD simulation as a tool to investigate mineralization mechanisms was dependable. The above simulation results can portray and reproduce the mineralization process to a certain extent, but they do not consider the effect of outer conditions and dispersion degree on the rate, as well as the effect of water film, and there are rare simulation studies on C_3S, which hinders the revelation of the mineralization mechanism of C_3S and the development of mineralization technology.

The composition of various industrial wastes is complex[20] and their impact on the mineralization mechanism is not valid nowadays. The rate of the reaction of CO_2 mineralization is influenced by many factors. Hence, to adjust the mineralization reaction overall, revealing the microscopic mineralization mechanism needs to be done. Due to this reason, the C_3S composite in industrial waste is taken as a mineralization resource to reveal the mineralization mechanism by RMD simulation in this work. The article is organized as follows: Section 2 provides a pithy description of RMD and force field validation results. Section 3 presents the simulation steps and parameters. The impact of outer conditions, dispersion degree, and water film on mineralization reaction dynamics and mechanism are expounded in Section 4. Conclusions are drawn in Section 5.

2. MATHEMATICAL MODEL

2.1. RMD Model. MD denotes the movement of molecules and atoms by Newton's Second Law. However, it is unable to model chemical reactions[21] and lacks the required accuracy.[22] On the other hand, quantum chemistry computation is rooted in the Schrödinger equation, which offers high accuracy but demands substantial computational resources. In contrast, RMD can represent the process of bond breaking and forming in the form of bond order.[23] It balances and transfers charge punctuation by the electron negativity. The equation is given by:

$$E_{\text{system}} = E_{\text{bond}} + E_{\text{over}} + E_{\text{angle}} + E_{\text{tors}} + E_{\text{vdWaals}} + E_{\text{Coulomb}} + E_{\text{Specific}} \quad (1)$$

where E_{system} is the total energy. E_{bond} is the bond forming energy between atoms as a continuous function of the distance between atoms. E_{angle} and E_{tors} are three-atom and four-atom dihedral energy, respectively. E_{over} is the revision term based on the atomic valence rule. E_{Coulomb} and E_{vdWaals} are the static charge energy and dispersion energy, respectively. E_{Special} is the term added to the definition for special systems.

The bond order of ReaxFF is calculated from an empirical formula.[24]

$$\begin{aligned} \text{BO}_{ij} &= \text{BO}_{ij}^{\sigma} + \text{BO}_{ij}^{\pi} + \text{BO}_{ij}^{n\pi} \\ &= \exp\left[p_{\text{bo1}}\left(\frac{r_{ij}}{r_{\text{o}}^{\sigma}}\right)^{p_{\text{bo2}}}\right] + \exp\left[p_{\text{bo3}}\left(\frac{r_{ij}}{r_{\text{o}}^{\pi}}\right)^{p_{\text{bot}}}\right] \\ &\quad + \exp\left[p_{\text{bo5}}\left(\frac{r_{ij}}{r_{\text{o}}^{\pi\pi}}\right)^{p_{\text{bob}}}\right] \end{aligned} \quad (2)$$

where BO_{ij} is the bond order between atoms i and j, r_{ij} is the distance between atoms i and j, r_{O} terms are the equilibrium bond lengths, and p_{bo} terms are empirical parameters.

The initial configuration was constructed from randomly placed molecules. In fact, the smaller the energy, the more stable the structure is. Therefore, the energy minimization process was conducted to make the model coordinate with the real situation. The equation of energy minimization is given by:

$$\begin{aligned} E(r_1, r_2, \cdots, r_N) &= \sum_{i,j} E_{\text{pair}}(r_i, r_j) + \sum_{ij} E_{\text{bond}}(r_i, r_j) \\ &\quad + \sum_{ijk} E_{\text{angle}}(r_i, r_j, r_k) + \\ &\quad \sum_{ijkl} E_{\text{dihedral}}\left(r_i, r_j, r_k, r_l\right) \\ &\quad + \sum_{ijkl} E_{\text{improper}}\left(r_i, r_j, r_k, r_l\right) + \sum_{i} E_{\text{fix}}(r_i) \end{aligned} \quad (3)$$

where $r_1, r_2, \cdots r_N$ are position vectors of atoms from 1 to N. E_{pair} is nonbonded pairwise bond interactions. E_{angle} is the bond angle interactions. E_{dihedral} is a dihedral interactions. E_{improper} is the improper dihedral interactions. E_{fix} is the extra energy term due to extra force to atoms. The left-hand side of the equation is the total energy of the system.

2.2. Model Validation. The RMD model must be validated before simulation. The force field parameters utilized were sourced from Joshi et al.[25] This study primarily focuses on validating bond length energy and angle energy, particularly

https://doi.org/10.1021/acsomega.4c07044
ACS Omega 2024, 9, 46237−46246

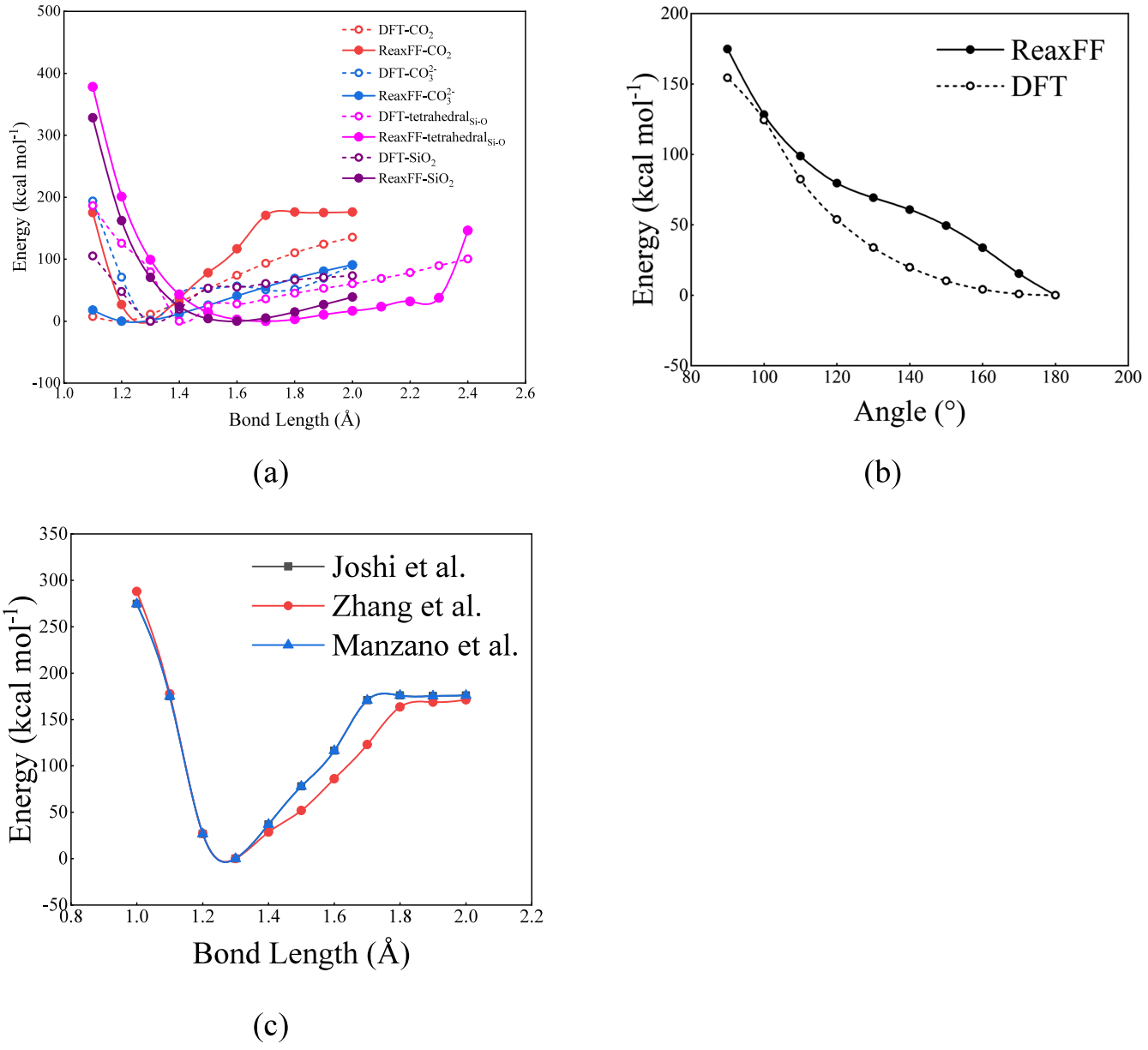

Figure 1. Model validation of force field: (a) bond length, (b) angle, and (c) different force fields. Dashed lines represent DFT results while solid lines represent ReaxFF results.

about CO_2 and carbonates. As depicted in Figure 1a, the DFT and ReaxFF results exhibit corresponding trends, and the location of the curve's extremal point is consistent between the two methods. It is worth noting that the bond energy calculated by ReaxFF deviates from that calculated by DFT when the bond length is less than the equilibrium length. However, this discrepancy is inconsequential, as it has a minimal impact on the simulation results. Figure 1b illustrates the O═C═O angle as a function of the angle, comparing the results between DFT and ReaxFF. The values at the same angle are very close to each other, and both methods yield minimum values at 180°. Figure 1c presents the results of the bond energy from different force fields.[25−27] These three types of force fields were applied in separate systems. The simulation results indicate that CO_2 bond energy is consistent among the three sources, suggesting that different force fields have a minimal impact on the simulation.

3. SIMULATION SETUPS

Figure 2 presents the simulation setup. The crystal cell is from the crystal database.[28] The crystal was built by repeating 8, 8,

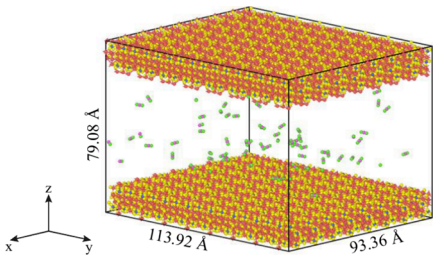

Figure 2. Model setup, where the blue sphere represents the silicon atom, the yellow sphere represents oxygen atoms of C_3S, the red sphere represents calcium atoms, the green sphere represents oxygen atoms of CO_2, and the magenta represents carbon atoms.

https://doi.org/10.1021/acsomega.4c07044
ACS Omega 2024, 9, 46237−46246

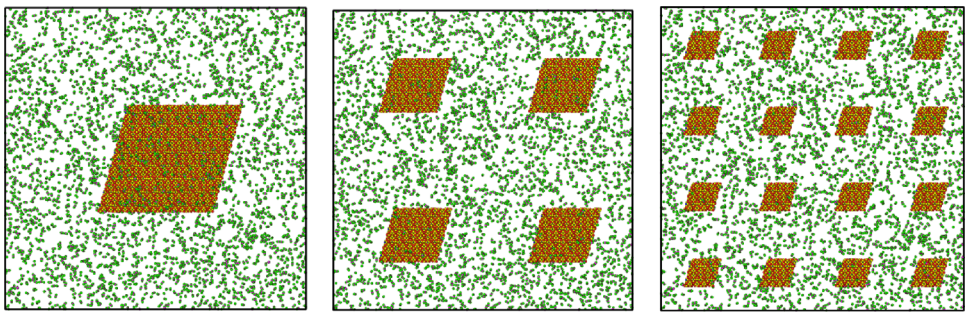

(a) (b) (c)

Figure 3. Model of different types of dispersion degree: (a) Compaction, (b) accumulation, and (c) spread.

and 2 times along the *x*, *y*, and *z* directions, respectively. The length along the *z* direction is 26.36 Å. The (001) surface[29] and $(00\bar{1})$ surface reacted with CO_2. The number of CO_2 molecules was calculated by volume and density as follows:

$$N = \frac{\rho V \times 10^3}{M} \times N_A \tag{4}$$

The models of different types of C_3S dispersion degrees are shown in Figure 3. The length of each periodic cubic box is 300 Å, and the number of CO_2 molecules is 3162. The mass of solids is equal to each other. The dispersion degree is represented as three kinds, spread, compaction, and accumulation. Dispersion degree decreases successively. The model of the C_3S surface covered by a water film is shown in Figure 4.

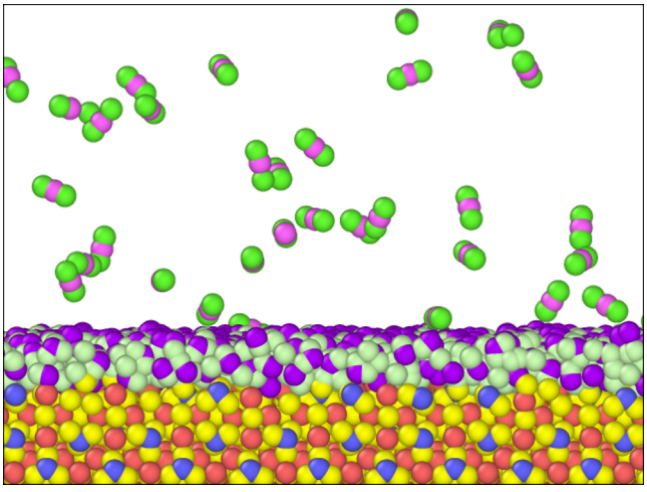

Figure 4. Model that the C_3S surface covered by the water film. Light green spheres represent hydrogen atoms and purple spheres represent oxygen of water.

Table 1 shows the simulation parameters. When the temperature is 298 K and the pressure is 0.5 MPa, the number of CO_2 molecules is 70. Energy minimization was conducted before formal simulation under a microcanonical ensemble (NVE). The size of the box was set to 93.36 Å × 113.92 Å × 79.08 Å. To research the impact of different parameters on reaction dynamics, the pressure range was set to 0.5−2.5 MPa and the temperature range to 298−358 K.

Table 1. Simulation Settings

simulation parameters	values
periodic conditions	*x*, *y*, *z*
box length along *x*, *y*, *z*	93.36 Å, 113.92 Å, 79.08 Å
temperature	298 K, 313 K, 328 K, 343 K, 358 K
pressure	0.5 MPa, 1.0 MPa, 1.5 MPa, 2.0 MPa, 2.5 MPa
ensemble	microcanonical ensemble (NVE)
temperature coupling algorithm	Berendsen
time step	0.25 fs
neighbor cut off for bond calculation	4.5 Å
H-bond cut off	6 Å

4. RESULTS AND DISCUSSION

4.1. CO_2 Mineralization Process. Figure 5 shows the mineralization process. The snapshots show the reaction of carbon dioxide molecules with C_3S. After the collision of activated CO_2 molecules with C_3S, the C═O bonds break up. C═O free radicals or O atoms bind to the tricalcium silicate crystal and form $CaCO_3$ and SiO_2. Meanwhile, the carbon atoms bind first in a few cases. Then, the left free radicals and atoms are adsorbed by C_3S. The ab initio MD of cleaved quartz carbonation revealed that CO_2 reacted with undercoordinated Si and nonbridging O atoms, thus forming CO_3, and was bonded to a solid surface by Si−O bonds.[30] When the time is 0.325 ps, the bond order between C and Ca is 2 and that between O and Ca is 0.966. When time is 0.775 ps, the bond order between C and Ca is 2. The bond order evolution of C═O is shown in Figure 6. Before the reaction, the bond order is near 2. When the time is 0.325 ps, the C═O breaks and the bond order is 0.

4.2. Effect of Temperature on Mineralization. Mean square displacements (MSD) have been widely employed to identify Brownian motion and random walk, which is a function of simulation time. The MSD is defined by[18]:

$$\mathrm{MSD} = \langle |r(t) - r(0)|^2 \rangle \tag{5}$$

where $r(t)$ represents the position coordination vector at time *t*; $r(0)$ represents the position coordination vector at initial time.

Figure 7 shows the effect of the temperature on the mineralization reaction rate. Within the time range of 0−9.7 ps, the MSD of 343 K is larger than that of all other temperatures. After 9.7 ps, the MSD of 358 K is bigger than 343 K. The MSD of 313 K is the lowest. Figure 7b shows the CO_2 molecules as a function of time at different temperatures.

https://doi.org/10.1021/acsomega.4c07044
ACS Omega 2024, 9, 46237−46246

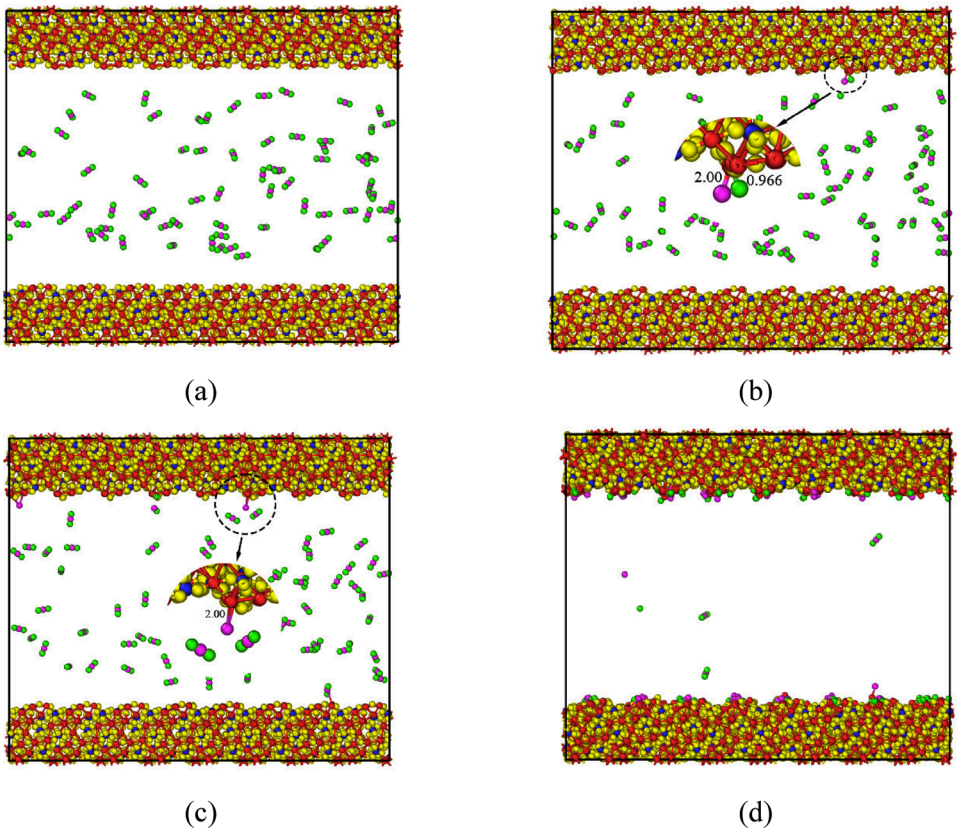

Figure 5. Mineralization process: Snapshots of (a) 0, (b) 0.325, (c) 0.775, and (d) 58.6 ps. The temperature is 313 K.

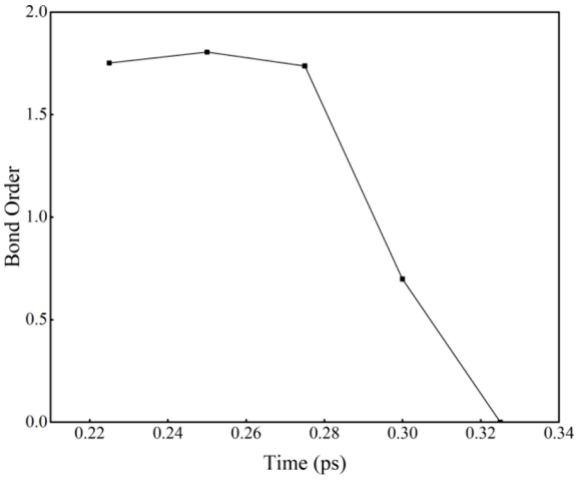

Figure 6. Bond order evolution of the C═O bond in the CO_2 molecule which is shown in Figure 5b.

It can be concluded from Figure 7b that the reaction of 298 K is slow, while that of other values is similar. CO_2 would adsorb on the C_3S surface and react with it during mineralization. High temperatures contributed to CO_2 getting away from the C_3S surface as a reverse process of adsorption. When the temperature was 313 K, the MSD of CO_2 reached the lowest because numerous CO_2 molecules were adsorbed on a solid surface, which constrained their free movement. It can be found from Figure 7b that the reaction is fast when the temperature is 328 K in 18−29 ps. In the late stage of the reaction, the MSD of 358 K is far higher than that of other temperatures because getting rid of adsorption becomes the main factor at this stage. It can be found from Figure 7b that the remaining CO_2 molecule number is just lower than that of 298 K within 14.8−31.9 ps. The MSD values are close to each other when the temperature is 298, 328, and 343 K.

The relationship between MSD and diffusion coefficient can be obtained by Einstein equation.[18]

$$D = \frac{\lim_{t\to\infty} \langle |r_i(t) - r_i(0)|^2 \rangle}{6t} \quad (6)$$

When the slope of the MSD curve is large, the diffusion coefficient is large. At each temperature, the slope of the MSD curves decreases as the reaction continues, which means diffusion coefficients are decreasing. Wang et al.[18] found that high temperatures contribute to a large slope. In this perspective, the situation is more complex. When the temperature is 358 K, the decreasing scale of the diffusion coefficient is big as time goes by. This is because many CO_2 molecules had been reacted in the late reaction stage and only a small quantity of them was adsorbed on the surface.

In the early stage of the reaction, the higher the temperature, the faster the mineralization reaction rate, which can also be concluded from Figure 8. However, the CO_2 molecules remain stable after 45 ps. The remaining numbers of CO_2 molecules at different temperatures are very close. Therefore, it contributes little to the mineralization conversion rate by raising the temperature. Nevertheless, temperature affects product form.[31]

4.3. Effect of Pressure on Mineralization. In the early stage of the reaction (0−29.0 ps), MSD decreases as pressure increases, except for that the values of 2.0 and 2.5 MPa are close. Because when pressure increases, in constant volume molecule number increases, the mean free range decreases. In

https://doi.org/10.1021/acsomega.4c07044
ACS Omega 2024, 9, 46237−46246

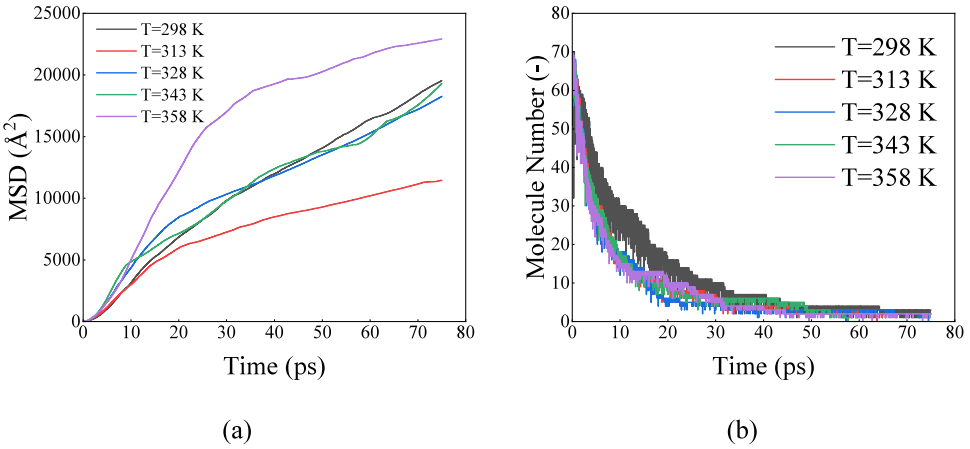

Figure 7. Effect of temperature on mineralization process: (a) CO_2 mean square displacement; (b) CO_2 molecule number.

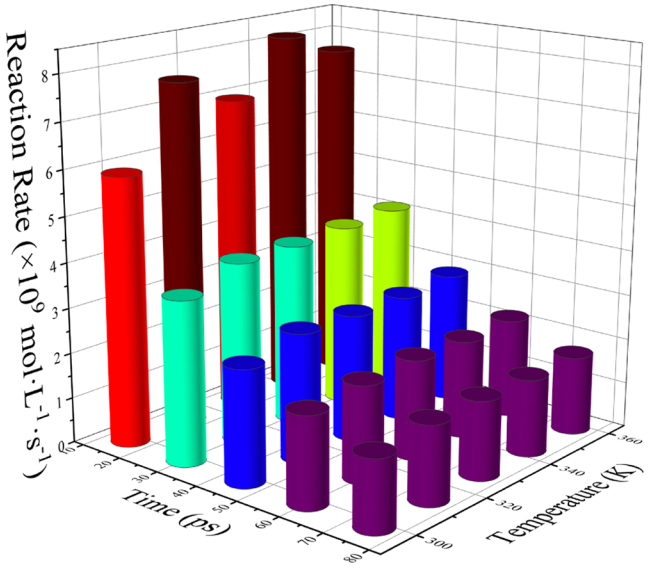

Figure 8. Average reaction rate as a function of the temperature at several time points.

the late stage of the reaction (29.0−71.9 ps), the MSD of 1.0 MPa is greater than that of 0.5 MPa. When pressure is 1.0 MPa, active CO_2 molecules can react with an active solid surface, and the left CO_2 molecules are not adsorbed. Therefore, the MSD is big. Figure 9b shows the CO_2 molecule number as a function of the simulation time. It can be found in Figure 9b that the conversion rate reaches the maximum when the pressure is 1.0 MPa, which is 96.6%.

The reaction rate increases as the pressure becomes higher, as seen in Figure 10. After 60 ps, the CO_2 molecule number reaches a stable value. However, when pressure is higher than 1 MPa, the mineralization conversion rate decreases. When pressure is 1.5, 2.0, and 2.5 MPa, the conversion rate decreases one by one.

4.4. Effect of Dispersion Degree on Mineralization.

Ashraf and Olek[32] pointed out that dispersing solid particles could contribute to gas reactions in the gap. The impact of dispersion degree on the mineralization reaction rate on the mechanism level is explained in this section. By simulation data that CO_2 molecule number changes as a function of time, it can be concluded that mineralization speed becomes fast as the dispersion degree increases.

It can be concluded from Figure 11a that the CO_2 molecule movement and diffusion are fast around the solid surface when dispersion degree is low. However, collision frequency decreases. The bigger the dispersion degree, the more access there is by CO_2 molecules. By raising the dispersion degree, the mineralization reaction rate can be raised. Berndsen[33] also pointed out that accessible area is one of the rate-limiting factors in mineralization.

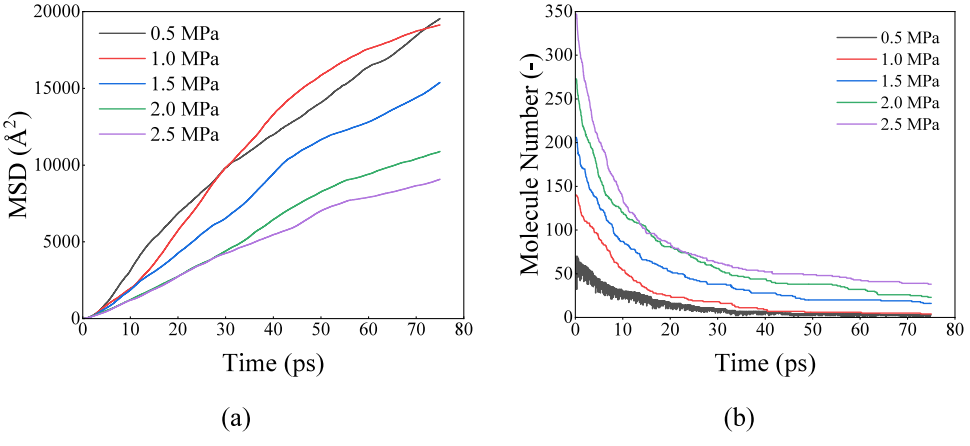

Figure 9. Pressure impaction on mineralization process: (a) CO_2 MSD and (b) CO_2 molecule number as a function of simulation time.

https://doi.org/10.1021/acsomega.4c07044
ACS Omega 2024, 9, 46237−46246

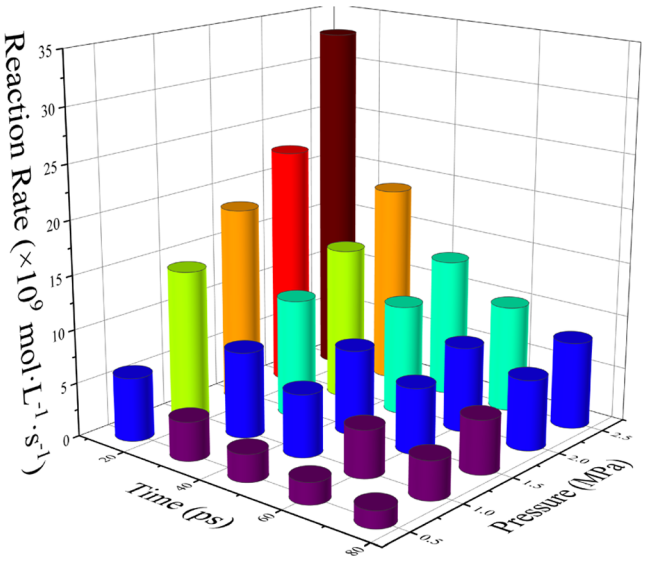

Figure 10. Average reaction rate as a function of the pressure at several time points.

Figure 11b shows the radial distribution function (RDF) of Ca and Si under different dispersion degrees, which can be calculated as follows.

$$g(r) = \frac{dN}{4\pi r^2 \rho dr} \tag{7}$$

dN is the atom number in the range from r to $r + dr$. ρ is the number density of atoms. RDF represents the distribution of the number density of one type of atom relative to another. The peak height represents the strength of the mutual interaction. It can be found that the peak of compact C_3S is the highest, while that of accumulated is in the middle. The peak height of spread C_3S is just 2/3 of compact since spread C_3S is taken by grinding solid and crystal structure is disrupted. The interaction strength between Ca and Si decreases, which contributes to CO_2 being adsorbed and enhances the mineralization reaction. The experiment of natural and industrial alkaline solids carbonation also illustrated that atomic topology is the rate-controlling step.[34] This is the same as the conclusion for accessible areas.

4.5. Effect of Water Film on Mineralization. In real mineralization reactions, there is usually a water film covering a solid in moist conditions.[15−17,35] Salah Uddin and Middendorf[36] pointed out that water tessellation was observed on the (001) surfaces of C_3S. The opposite surface $(00\bar{1})$ has no spontaneous reactive site.[37] Thus, based on Figure 2, the model with water film covered on (001) surface was constructed, which is shown in Figure 4. The hydration process of C_3S can be expressed as[38]:

$$Ca_3SiO_5 + 5.2H_2O \rightarrow 1.2Ca(OH)_2 + (CaO)_{1.8}SiO_2(H_2O)_{4.0} \tag{8}$$

The difference in reaction speed with and without a water film is obvious, as shown in Figure 12a. Without water, the CO_2 conversion rate is 95.7%, while it is only 84.3% with water. Without water, the molecular number of CO_2 stays constant after 45.8 ps. From the initial state to this point, the average reaction speed of CO_2 is 4.27×10^9 mol/(L s), while it is 3.82×10^9 mol/(L s) with water. Water film covered in the solid surface has a negative influence on mass transfer during mineralization, and the reaction rate and conversion rate will decrease, which is in coordination with others' work simulated by the ab initio MD method.

Figure 12b demonstrates the reaction path of mineralization with water. In the early stage (0−3.1 ps), C_3S hydration occurs, and numerous $Ca(OH)_2$ is produced. The dissolution of OH^- can provide an alkaline environment for mineralization. This is usually called the alkali activation phenomenon. $Ca(OH)_2$ dissolves in water and much OH^- comes into being. However, OH^- is run out quickly. Water molecules decrease very quickly since C_3S is the active hydration solid phase and the water film is directly covered on its surface. The number of water molecules is 142 at first and decreases to 18 at 7.0 ps. About 87.3% of water molecules participate in the reaction. Water molecules decrease to 8 at 21.1 ps and remain stable afterward.

Figure 13 shows the coordination number of Si atoms around Ca. The coordination is calculated from the surface layer of C_3S with a depth of 5 Å. At the initial state, the coordination number is around 8 and then decreases. Li et al.[39] also pointed out that the connectivity between Ca and Si can be up to eight. As the reaction progresses, $CaSiO_3$ turns into $CaCO_3$. Thus, the coordination number of Si around Ca decreases as time goes by.

In conclusion, although the water film contributes to the alkali activation phenomenon and OH^- is produced, OH^- runs

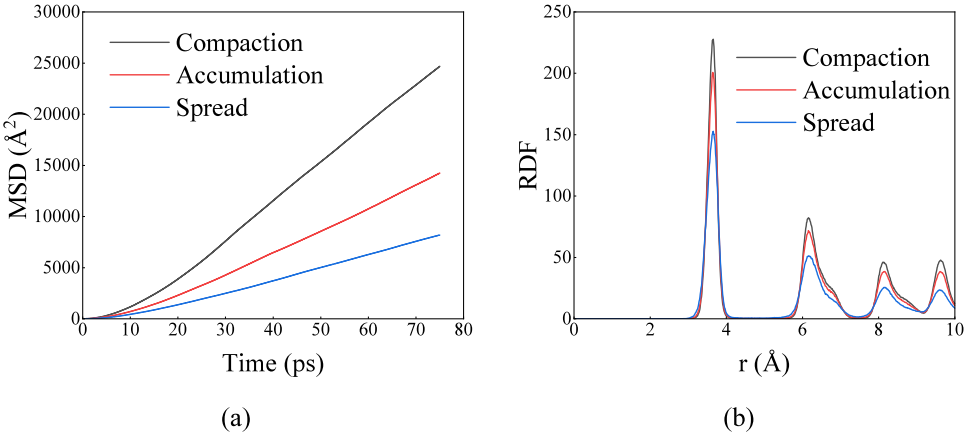

Figure 11. Comparison among different types of solid dispersion degree. (a) MSD. (b) RDF of Ca and Si.

https://doi.org/10.1021/acsomega.4c07044
ACS Omega 2024, 9, 46237−46246

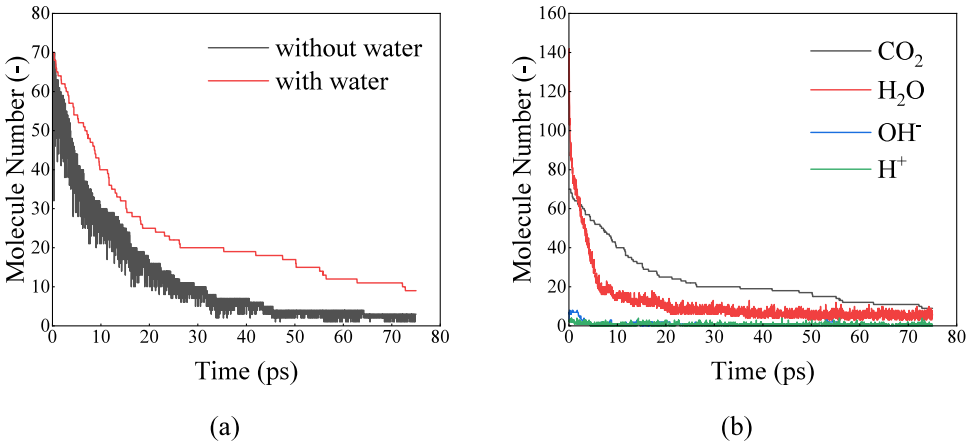

Figure 12. Molecule number as a function of time: (a) CO_2 molecule number with and without water and (b) molecule number during reaction.

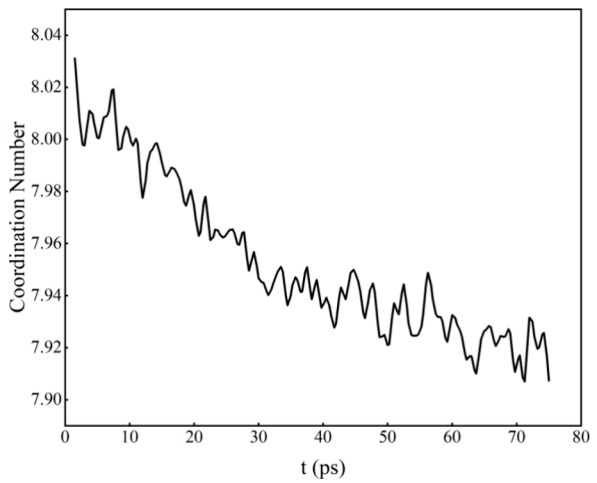

Figure 13. Coordination number of Si atoms around Ca varies with time.

out within just 3.1 ps. The negative effect of water that hinders the diffusion of CO_2 to a solid surface is during the process, which takes more effect. In a word, water film decreases the mineralization reaction rate and conversion rate. Falzone[40] also pointed out that the drying process is necessary before and during mineralization.

4.6. Discussion. CO_2 mineralization reactions are affected by many factors, including inner and outer ones. This article focuses on temperature and pressure as outer factors and dispersion degree as inner factors. Temperature has two opposite effects on mineralization reaction dynamics. On the one hand, high temperature activates reactants and accelerates reaction. On the other hand, high temperature contributes to adsorbed CO_2 molecules getting rid of the C_3S surface, which is not conducive to reaction dynamics. This work takes the active solid phase components, C_3S to carry out research. In reality, industrial wastes contain many crystalline phases, which makes the reaction speed not as fast as this work. The temperature of 328 K is the best choice for industrial wastes whose main reactive solid phase is C_3S. Polettini et al.[10] also pointed out that the optimum temperature for BOF slag is 50 °C by experiment, which is very close to the results in this article. High pressure made the reaction fast. However, higher pressures require reaction vessels with higher pressure capacities. In this way, the right pressure needs to be selected to save production costs. Grinding and pulverizing industrial solid waste can increase the dispersion degree. High dispersion degree not only activates the solid phase but also increases the effective specific surface area for the gas−solid reaction. When mineralization is under moisture conditions, solid waste is usually covered by a layer of water film. Water promotes the phenomenon of alkali excitation in the early stage. However, the hydroxide ions produced are consumed in a very short period. The water film limits the direct contact of CO_2 molecules with C_3S. This effect is throughout the whole reaction. Thus, the reaction rate and conversion rate decrease in general. RMD saves computational costs for simulating mineralization reactions compared with the DFT and AIMD methods. Thus, it can simulate a long period and reveal many aspects of mineralization. However, its accuracy relies on the force field. The model built in this article simulates direct mineralization. Usually, indirect mineralization is widely used in industry. Because the reaction condition is mild, the energy cost is low. In the future, indirect mineralization should be considered to be researched. The reaction dynamics investigated in this review can guide industrial practice.

5. CONCLUSIONS

By RMD simulation, the CO_2 mineralization reaction dynamics is investigated in this article. The model is composed of a C_3S solid and CO_2 gas. The influence of temperature and pressure is investigated. Also, the water film is added in one section to show its role in the reaction. This research work is expected to provide theoretical guidance for quantitative regulation of industrial production. Based on the results, several conclusions can be drawn:

1. Temperature has a dual effect on the kinetics of the mineralization reaction. Elevating the temperature increases the reactant activity but also promotes the detachment of carbon dioxide molecules from the surface of the C_3S solid phase. In terms of increasing the reaction rate, 328 K is the best choice.
2. Increasing pressure increases collision frequency and enhances reaction. The higher the pressure, the faster the reaction rate. In actual industrial production, the cost increase of increasing the pressure needs to be taken into account to determine the optimal pressure.
3. Grinding and pulverizing solid waste are often employed in engineering. The dispersion degree of the solid phase is classified into three types: compaction, accumulation,

https://doi.org/10.1021/acsomega.4c07044
ACS Omega 2024, 9, 46237−46246

and spread in this article. By raising the dispersion degree, the crystal structure of the solid phase is ruined and reactivity is enhanced. Moreover, the effective access area is increased. Therefore, increasing the dispersion degree can reinforce the mineralization reaction.

4. In moisture conditions, the C_3S solid surface is usually covered with a layer of water film. The coordination number of Si surrounding Ca on the surface of C_3S was analyzed. During the reaction, C_3S turned into $CaCO_3$. Thus the coordination number decreased. Water facilitates the alkali excitation phenomenon and drives C_3S to produce a large amount of OH^- in a short period. However, the OH^- ions are consumed shortly, and the negative effect of water film that prevents direction access of CO_2 and C_3S is throughout the entire process. Generally, the reaction rate and conversion rate decrease with water film. In the real mineralization process, keeping the environment dry can contribute to the process of reaction.

AUTHOR INFORMATION

Corresponding Author

Kun Luo − *State Key Laboratory of Clean Energy Utilization, Zhejiang University, Hangzhou 310027, China; Shanghai Institute for Advanced Study of Zhejiang University, Shanghai 200120, China;* orcid.org/0000-0003-3644-9400; Email: zjulk@zju.edu.cn

Authors

Erchao Li − *State Key Laboratory of Clean Energy Utilization, Zhejiang University, Hangzhou 310027, China*

Jianan Zheng − *Shanghai Institute for Advanced Study of Zhejiang University, Shanghai 200120, China;* orcid.org/0000-0003-4022-3017

Junjie Lin − *State Key Laboratory of Clean Energy Utilization, Zhejiang University, Hangzhou 310027, China*

Tao Wang − *State Key Laboratory of Clean Energy Utilization, Zhejiang University, Hangzhou 310027, China;* orcid.org/0000-0002-0535-7821

Jianren Fan − *State Key Laboratory of Clean Energy Utilization, Zhejiang University, Hangzhou 310027, China; Shanghai Institute for Advanced Study of Zhejiang University, Shanghai 200120, China;* orcid.org/0000-0002-6332-6441

Complete contact information is available at: https://pubs.acs.org/10.1021/acsomega.4c07044

Notes

The authors declare no competing financial interest.

ACKNOWLEDGMENTS

We are grateful for the support from the Zhejiang Provincial Natural Science Foundation of China (Grant No. LDT23E06013E06).

REFERENCES

(1) Mikhaylov, A; Moiseev, N; Aleshin, K; Burkhardt, T Global climate change and greenhouse effect. *JESI* **2020**, *7*, 2897−2913.

(2) Schloesser, F; Friedrich, T; Timmermann, A; DeConto, R. M.; Pollard, D Antarctic iceberg impacts on future Southern Hemisphere climate. *Nat Clim Chang* **2019**, *9*, 672−677.

(3) Dziejarski, B; Krzyżyńska, R; Andersson, K Current status of carbon capture, utilization, and storage technologies in the global economy: A survey of technical assessment. *Fuel* **2023**, *342*, No. 127776.

(4) Pan, S-Y; Chen, Y-H; Fan, L-S; Kim, H; Gao, X; Ling, T-C; et al. CO2 mineralization and utilization by alkaline solid wastes for potential carbon reduction. *Nat Sustain* **2020**, *3*, 399−405.

(5) Zheng, X; Liu, J; Wang, Y; Wang, Y; Ji, L; Yan, S Regenerable glycine induces selective preparation of vaterite CaCO3 by calcium leaching and CO2 mineralization from coal fly ash. *Chemical Engineering Journal* **2023**, *459*, No. 141536.

(6) Verduyn, M; Geerlings, H; Mossel, G. V.; Vijayakumari, S Review of the various CO2 mineralization product forms. *Energy Procedia* **2011**, *4*, 2885−2892.

(7) Lackner, K. S. A Guide to CO2 Sequestration. *Science* **2003**, *300*, 1677−1678.

(8) Reddy, K. J.; John, S; Weber, H; Argyle, M. D.; Bhattacharyya, P; Taylor, D. T.; et al. Simultaneous capture and mineralization of coal combustion flue gas carbon dioxide (CO2). *Energy Procedia* **2011**, *4*, 1574−1583.

(9) Helwani, Z; Wiheeb, A. D.; Kim, J; Othman, M. R. In-situ mineralization of carbon dioxide in a coal-fired power plant. *Energy Sources, Part A: Recovery, Utilization, and Environmental Effects* **2016**, *38*, 606−611.

(10) Polettini, A; Pomi, R; Stramazzo, A CO2 sequestration through aqueous accelerated carbonation of BOF slag: A factorial study of parameters effects. *Journal of Environmental Management* **2016**, *167*, 185−195.

(11) Cheng, C; Huang, W; Xu, H; Liu, Z; Li, X; Shi, H; et al. CO2 sequestration and CaCO3 recovery with steel slag by a novel two-step leaching and carbonation method. *Science of The Total Environment* **2023**, *891*, No. 164203.

(12) Said, A; Mattila, H-P; Järvinen, M; Zevenhoven, R Production of precipitated calcium carbonate (PCC) from steelmaking slag for fixation of CO2. *Applied Energy* **2013**, *112*, 765−771.

(13) Sun, M; Geng, G; Xin, D; Zou, C Molecular quantification of the decelerated dissolution of tri-calcium silicate (C3S) due to surface adsorption. *Cem. Concr. Res.* **2022**, *152*, No. 106682.

(14) Zhao, M; Lu, L; Tao, Y; He, Y; Wang, F; Zhang, W; et al. Adsorption behavior of carbonic acid on γ-dicalcium silicate surface from molecular simulations. *J. Am. Ceram. Soc.* **2022**, *105*, 564−576.

(15) Mutisya, S. M.; Kalinichev, A. G. Carbonation Reaction Mechanisms of Portlandite Predicted from Enhanced Ab Initio Molecular Dynamics Simulations. *Minerals* **2021**, *11*, 509.

(16) Zare, S; Funk, A; Abdolhosseini Qomi, M. J. Formation and Dissolution of Surface Metal Carbonate Complexes: Implications for Interfacial Carbon Mineralization in Metal Silicates. *J Phys Chem C* **2022**, *126*, 11574−11584.

(17) Qin, L; Mao, X; Cui, Y; Bao, J; Sant, G; Chen, T; et al. New insights into the early stage nucleation of calcium carbonate gels by reactive molecular dynamics simulations. *J. Chem. Phys.* **2022**, *157*, 234501.

(18) Wang, N; Feng, Y; Guo, X; van Duin, A. C. T. Insights into the Role of H2O in the Carbonation of CaO Nanoparticle with CO2. *The Journal of Physical Chemistry C* **2018**, *122*, 21401−21410.

(19) Dai, X; Wei, C; Wang, M; Zhang, J; Wang, X; Shi, X; et al. Understanding CO2 mineralization and associated storage space changes in Illite using molecular dynamics simulation and experiments. *Energy* **2023**, *283*, No. 128467.

(20) Pan, S-Y; Adhikari, R; Chen, Y-H; Li, P; Chiang, P-C Integrated and innovative steel slag utilization for iron reclamation, green material production and CO2 fixation via accelerated carbonation. *Journal of Cleaner Production* **2016**, *137*, 617−631.

(21) Chmiela, S; Sauceda, H. E.; Müller, K-R; Tkatchenko, A Towards exact molecular dynamics simulations with machine-learned force fields. *Nat Commun.* **2018**, *9*, 3887.

(22) Wan, S; Sinclair, R. C.; Coveney, P. V. Uncertainty quantification in classical molecular dynamics. *Phil. Trans. R. Soc. A* **2021**, *379*, 20200082.

(23) Senftle, T. P.; Hong, S; Islam, M. M.; Kylasa, S. B.; Zheng, Y; Shin, Y. K.; et al. The ReaxFF reactive force-field: development, applications and future directions. *npj Comput. Mater.* **2016**, *2*, 15011.
(24) Russo, M. F.; Van Duin, A. C. T. Atomistic-scale simulations of chemical reactions: Bridging from quantum chemistry to engineering. *Nuclear Instruments and Methods in Physics Research Section B: Beam Interactions with Materials and Atoms* **2011**, *269*, 1549−1554.
(25) Joshi, K. L.; Psofogiannakis, G.; van Duin, A. C. T.; Raman, S. Reactive molecular simulations of protonation of water clusters and depletion of acidity in H-ZSM-5 zeolite. *Phys. Chem. Chem. Phys.* **2014**, *16*, 18433−18441.
(26) Zhang, Y; Zhou, Q; Ju, J. W.; Bauchy, M New insights into the mechanism governing the elasticity of calcium silicate hydrate gels exposed to high temperature: A molecular dynamics study. *Cem. Concr. Res.* **2021**, *141*, No. 106333.
(27) Manzano, H; Pellenq, R. J. M.; Ulm, F-J; Buehler, M. J.; Van Duin, A. C. T. Hydration of Calcium Oxide Surface Predicted by Reactive Force Field Molecular Dynamics. *Langmuir* **2012**, *28*, 4187−4197.
(28) Golovastikov, N.; Matveeva, R.; Belov, N. Crystal structure of tricalcium silicate, 3CaO.SiO2 = C3S, 1975.
(29) Lee, M.-S.; Peter McGrail, B.; Rousseau, R.; Glezakou, V.-A. Structure, dynamics and stability of water/scCO2/mineral interfaces from ab initio molecular dynamics simulations. *Sci. Rep.* **2015**, *5*, No. 14857.
(30) Jia, J.; Lian, Y.; Tsuji, T.; Miranda, C. R.; Masuda, Y.; Matsuoka, T. Ab lnitio Molecular Dynamics Study of Carbonation and Hydrolysis Reactions on Cleaved Quartz (001) Surface. *J. Phys. Chem. C* **2019**, *123*, 4938−4948.
(31) Liu, P.; Chen, Y.; Yu, Z.; Zhang, R. Effect of Temperature on Concrete Carbonation Performance. *Adv. Mater. Sci. Eng.* **2019**, *2019*, 1−6.
(32) Ashraf, W; Olek, J Carbonation behavior of hydraulic and non-hydraulic calcium silicates: potential of utilizing low-lime calcium silicates in cement-based materials. *J. Mater. Sci.* **2016**, *51*, 6173−6191.
(33) Berndsen, M; Erol, S; Akın, T; Akın, S; Nardini, I; Immenhauser, A; et al. Experimental study and kinetic modeling of high temperature and pressure CO2 mineralization. *International Journal of Greenhouse Gas Control* **2024**, *132*, No. 104044.
(34) La Plante, E. C.; Mehdipour, I; Shortt, I; Yang, K; Simonetti, D; Bauchy, M; et al. Controls on CO2 mineralization Using Natural and Industrial Alkaline Solids under Ambient Conditions. *ACS Sustainable Chemistry & Engineering* **2021**, *9*, 10727−10739.
(35) Abdolhosseini Qomi, M. J.; Miller, Q. R. S.; Zare, S; Schaef, H. T.; Kaszuba, J. P.; Rosso, K. M. Molecular-scale mechanisms of CO2 mineralization in nanoscale interfacial water films. *Nat Rev Chem* **2022**, *6*, 598−613.
(36) Salah Uddin, K; Middendorf, B Reactivity of Different Crystalline Surfaces of C3S During Early Hydration by the Atomistic Approach. *Materials* **2019**, *12*, 1514.
(37) Manzano, H; Durgun, E; López-Arbeloa, I; Grossman, J. C. Insight on Tricalcium Silicate Hydration and Dissolution Mechanism from Molecular Simulations. *ACS Appl Mater Interfaces* **2015**, *7*, 14726−14733.
(38) Cuesta, A.; Zea-Garcia, J. D.; Londono-Zuluaga, D.; De La Torre, A. G.; Santacruz, I.; Vallcorba, O.; et al. Multiscale understanding of tricalcium silicate hydration reactions. *Sci. Rep.* **2018**, *8*, 8544.
(39) Li, J; Zhang, W; Garbev, K; Monteiro, P. J. M. Coordination environment of Si in calcium silicate hydrates, silicate minerals, and blast furnace slags: A XANES database. *Cem. Concr. Res.* **2021**, *143*, No. 106376.
(40) Falzone, G; Mehdipour, I; Neithalath, N; Bauchy, M; Simonetti, D; Sant, G New insights into the mechanisms of carbon dioxide mineralization by portlandite. *AIChE J.* **2021**, *67*, No. e17160.

https://doi.org/10.1021/acsomega.4c07044
ACS Omega 2024, 9, 46237−46246